

Low energy crossed beam studies of OD^+ and D_2O^+ with C_2H_4 : covalent and electrostatic complexes

Li Liu¹, Yue Li^{1,2}, Xiaohui Cai^{1,3}, Elizabeth S Richards¹ and James M Farrar¹

¹ Department of Chemistry, University of Rochester, Rochester, NY 14627, USA

E-mail: farrar@chem.rochester.edu

Received 9 April 2007

Accepted for publication 20 June 2007

Published 3 August 2007

Online at stacks.iop.org/PhysScr/76/C48

Abstract

Density functional theory (DFT) calculations are used in conjunction with low-energy crossed beam studies of the ion-molecule reactions of D_2O^+ and OD^+ with C_2H_4 to probe collision dynamics, particularly the role that electrostatic and covalent intermediates play. In the D^+ -transfer reaction initiated with D_2O^+ , an electrostatic complex formed when the transferred species approaches the perpendicular bisector of the $\text{C}=\text{C}$ bond plays an important role. Observation of $\text{C}_2\text{H}_4\text{D}^+$ products with excitation in the ν_{10} stretching mode, in which the bridging D-atom moves along the perpendicular bisector, provides support for this complex. In the OD^+ reaction, evidence for the occurrence of reaction on the ground singlet surface following internal conversion comes from the observation of a transient complex living ~ 100 fs. The DFT calculations show that the rate-limiting step corresponds to ring-opening and H/D exchange initiated in an ethylene oxide species with D^+ bound to the oxygen atom. Computed lifetimes are in agreement with experiment. This study provides an example of how high-resolution crossed beam studies in conjunction with quantum chemical calculations, can provide a detailed understanding of collision dynamics in systems of moderate complexity. New experimental developments, including the application of velocity space imaging methods, as well as the production of beams of free radicals, will lead to a greater understanding of energy and angular momentum disposal in systems of chemical relevance.

PACS numbers: 82.20.Bc, 82.20.Hf, 82.20.Kh, 82.30.Fi

(Some figures in this article are in colour only in the electronic version.)

1. Introduction

The role of the long-range attractive interaction between a gas phase ion and an atomic or molecular collision partner has been a primary focus of experimental and theoretical studies of such systems. Although electrostatic interactions alone generally allow one to calculate rate constants for ion-neutral reactions with quantitative accuracy [1], it has been appreciated for some time that understanding more

detailed questions of collision dynamics, i.e. ‘where the energy goes in a chemical reaction’ [2], requires us to understand the motion of the collision system not only in the long range regime where the initial electrostatically bound encounter complex is formed, but also over extended regions of the system’s full potential energy surface. However, no general method exists for systematically probing the potential energy surface, a function of the $3N-6$ internal coordinates. Significant progress has been made for three-atom systems [3–5] but detailed experimental and theoretical treatments even for four-atom systems are very limited in scope [6]. Experimentally, approaches to probing potential energy surfaces have been based on control of collision

² Present address: Department of Chemistry, George Washington University, Washington, DC, USA

³ Present address: Department of Chemistry, University of Houston, Houston, TX 77004, USA

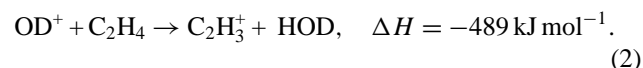
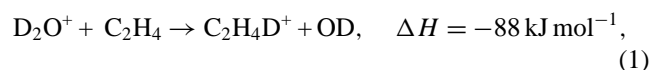
energy, systematic variation of molecular complexity, and attention to kinematic restrictions [7]. More generally, variations in reactant mass ratios, which result in systematic variations in the skew angle β of the potential energy surface expressed in scaled and skewed coordinates [8] can also give insight into features of the potential energy surface that control energy disposal. For example, early work by Mahan [9, 10] and more recent elaborations by Valentini and co-workers [11] have explored the role of kinematics and the locations and magnitudes of potential energy barriers in controlling energy disposal in reactions of significant complexity.

The role that collision complexes play in energy disposal and in determining the timescale for reaction is a topic with a long history in collision dynamics. Pioneering work by Herschbach [12], Bernstein [13], Kinsey [14] and their co-workers established the importance of angular momentum disposal and complex geometry in determining product angular distributions in reactions governed by a transient complex. In favorable cases, the rotational period of the complex serves as a ‘clock’, allowing direct determinations of the timescale for collision processes. Theoretical treatments of product kinetic energy distributions in terms of phase space theory [15, 16] have also played an important role in assessing the statistical nature of energy partitioning when transient complexes decay. The statistical character of product energy partitioning is a topic that remains at the forefront of crossed beam studies of elementary reaction dynamics.

The crossed beam method [17, 18], one of a number of techniques that have been developed over the past few decades to probe collision mechanics under single collision conditions, has played an important role in understanding features of the potential energy surface that governs reaction, as the examples in the preceding paragraphs have demonstrated. Improvements in reactant preparation and product detection have been responsible for many of the advances of this technique [19–21]. With modern methods of quantum chemistry, it is now possible to compute the energies and geometries of key reactive intermediates in systems of significant complexity; furthermore, determining the vibrational energy levels of these intermediates and the transition states connecting them allow one to compute isomerization rates. Under favorable conditions, crossed beam studies of such systems can probe rate-limiting isomerization processes and energy disposal in a manner that allows direct comparison of theory and experiment.

This comment focuses on the synergy between experimental studies of the reactions of the cations OD^+ and D_2O^+ with the ethylene molecule, C_2H_4 , and density functional theory (DFT) calculations of key intermediates and transition states connecting them. These processes probe both the relatively simple process of light atom transfer, as well as the more complex process of electrophilic addition to carbon–carbon double bonds. The calculations provide information about preferred reaction geometries and intermediate lifetimes that experiments probe directly via product energy disposal and angular distributions. The synergy between theory and experiment in these systems of moderate complexity suggests that insight into the nature of reactive pathways in more complex gas phase processes can be facilitated by such treatments.

The reactions that we report on are the following:



Aside from charge transfer, these reactions are the major reactive channels. Complete studies of the OD^+ and D_2O^+ systems have appeared in the literature [22, 23].

2. Experimental

The crossed beam instrument has been described in detail in previous publications [24]. OD^+ and D_2O^+ ions were produced by electron impact on deuterium oxide vapour in an ion source held at a pressure of approximately 0.01 Torr. Following extraction, the ions were accelerated to 300 eV, and were then mass-selected by a 60° magnetic sector. After focusing and deceleration to the desired beam energy by a series of ion optics, the beam had a roughly triangular kinetic energy distribution characterized by a full width half-maximum (FWHM) between 0.20 and 0.45 eV in the laboratory frame of reference.

Experiments were performed at selected energies over a relative collision energy range from 0.20 to 1.06 eV (19.3–102 kJ mol⁻¹). This five-fold range was sufficient to access both attractive and low energy repulsive components of the full potential energy surfaces of these systems. Ethylene beams were formed by supersonic expansion of the pure gas through a 0.07 mm nozzle. After passing through a 1.0 mm diameter skimmer, the beam was collimated, and then entered the main chamber, where it intersected the ion beam at a 90° angle. A tandem electrostatic energy analyser with resolution of 0.07 eV and quadrupole mass filter determined the kinetic energies and masses of ions in the primary ion beam and scattered ionic reaction products. The energy analyser was calibrated before and after the experiments by measuring the kinetic energy distribution of thermal ions formed by resonant charge transfer between He^+ and He. The energy- and mass-analysed product ions were detected with dual microchannel plates. A schematic of the instrument is shown in figure 1.

3. Results

Kinetic energy scans of the reactively scattered product flux were transformed to the center-of-mass coordinate system using the iterative deconvolution method of Siska [25]. Figures 2 and 3 show selected velocity space images of the center-of-mass flux distribution for the products of reactions (1) and (2). The most salient aspect of the flux image for the formation of $\text{C}_2\text{H}_4\text{D}^+$ via reaction (1), shown in figure 2, is the fact that the distribution is strongly asymmetric with respect to the centroid, and shows weak structure that corresponds to the formation of products with specific number of quanta in selected vibrations. The formation of C_2H_3^+ via reaction (2), shown in figure 3, is also asymmetric with respect to the centroid, but does show a weak peak in the backward direction, indicating that the collision is ‘sticky’, i.e., involves a transient complex living a fraction of a rotational period that provides important insight into the lifetime of a key intermediate complex.

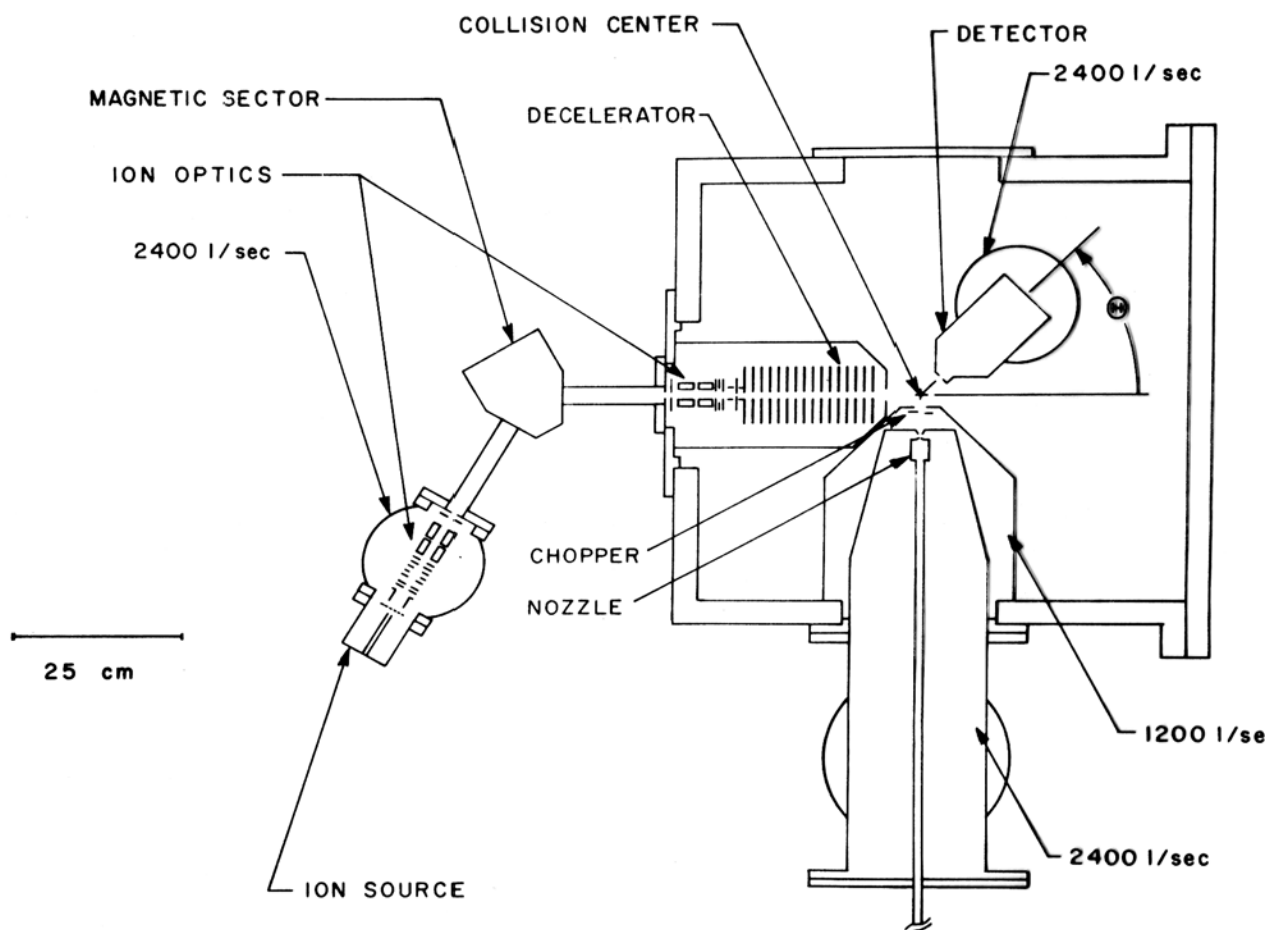


Figure 1. Schematic diagram of crossed beam instrument.

Integration of these flux distributions over center-of-mass speed yields product angular distributions according to the following equation:

$$g(\theta) = \int_0^{\infty} I_{\text{c.m.}}(u, \theta) du. \quad (3)$$

Similarly, the angle-averaged relative translational energy distributions of products, $P(E_{T'})$, are calculated by integrating the c.m. intensity over the appropriate angular range:

$$P(E_{T'}) = \int_0^{\pi} u^{-1} I_{\text{c.m.}}(u, \theta) \sin \theta d\theta. \quad (4)$$

These distributions provide additional insight into the dynamics of reactive collisions. In figure 4, we show the kinetic energy distributions for the formation of $\text{C}_2\text{H}_4\text{D}^+$ formed by reaction (1). The distribution at the lowest collision energy, 0.34 eV, is unstructured, with the mean kinetic energy of the products equal to 0.36 eV. At the next collision energy, 0.55 eV, the distribution has shifted to higher translational energies, corresponding to a mean energy of 0.53 eV, and reproducible structure appears in the distribution. At the highest collision energy of 0.78 eV, the product translational energy distribution has again shifted upward, the mean energy increasing to 0.74 eV. At all three collision energies, the

mean product internal energy is 0.92 ± 0.03 eV (89 kJ mol^{-1}), equal to the reaction exothermicity within experimental error. The structure in the kinetic energy distributions that was first observed at 0.55 eV collision energy persists at this energy. In figure 4, a set of vertical lines with a spacing of 0.19 eV provides a reasonable fit to the oscillations in the kinetic energy distributions. The observation of these periodic oscillations, which is facilitated by favorable kinematics and low product rotational excitation, is correlated with the formation of products with discrete numbers of quanta in specific vibrations. The theoretical calculations described in the next section will assist us in understanding which product vibrations are likely to be associated with this structure in the kinetic energy distributions.

In figure 5, we show the angular and kinetic energy distributions for C_2H_3^+ formed by reaction (2). The kinetic energies shift toward higher energies with increasing collision energy; the hydride transfer reaction is quite exothermic, so the fraction of the available energy in translation is relatively small for a particle transfer reaction, ranging from 5.5 to 16%. However, the angular distributions convey the most interesting insight into the reaction. At the lowest collision energy, products are peaked both in the forward and backward hemispheres. Such an angular distribution is consistent with the modulation of the $1/\sin \theta$ form factor associated with the decay of a prolate symmetric top [12] by a random distribution

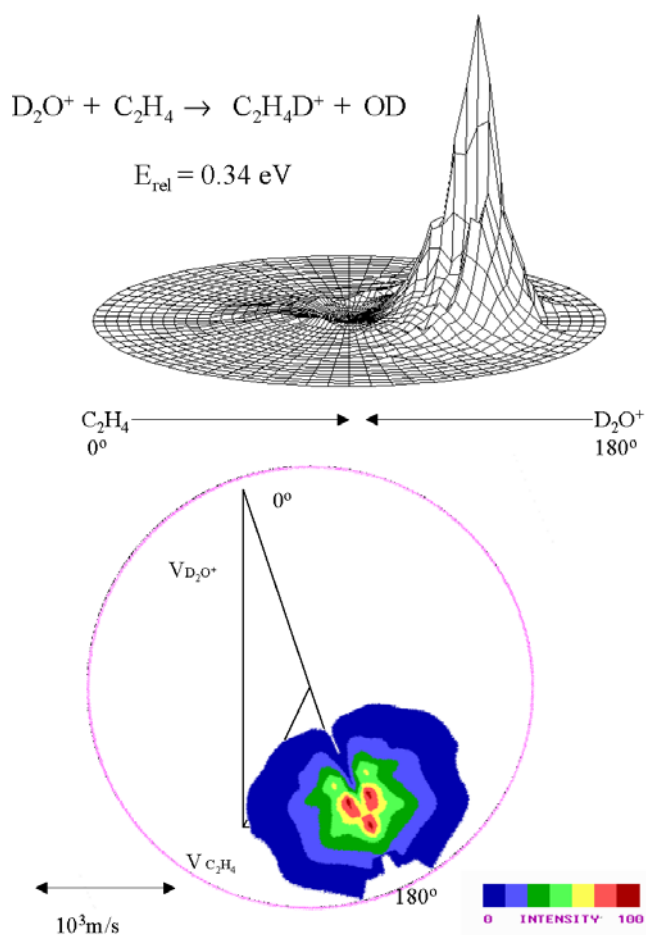


Figure 2. Top panel: axonometric representation of the $\text{C}_2\text{H}_4\text{D}^+$ product flux in velocity space from the reaction of D_2O^+ and C_2H_4 , 0.34 eV (32.8 kJ mol^{-1}). Bottom panel: contour plot representation of the $\text{C}_2\text{H}_4\text{D}^+$ product flux superimposed on the Newton diagram. The circle denotes the maximum $\text{C}_2\text{H}_4\text{D}^+$ product velocity allowed by energy conservation. Reprinted from [22] with permission of the American Institute of Physics.

of lifetimes comparable to or shorter than the complex's rotational period.

4. Computations

Quantum chemical calculations of the energies and structures of key reactive intermediates and transition states for reactions (1) and (2) were performed with DFT calculations via the Gaussian 98 program package. The objective of these calculations was to identify key reactive intermediates and their rates of formation and interconversion at total energies consistent with the collision energies of these experiments. The geometries of all the relevant species were fully optimized at the B3LYP/6-311+G* level. Vibrational frequencies of intermediates and transition states were computed in the harmonic approximation. Single point energy calculations were performed at the same level of theory based on the geometries and zero-point vibrational energies. Intermediate complex and transition state structures and vibrational energy levels were used as input to statistical Rice–Ramsperger–Kassell–Marcus (RRKM) rate constant calculations [26, 27].

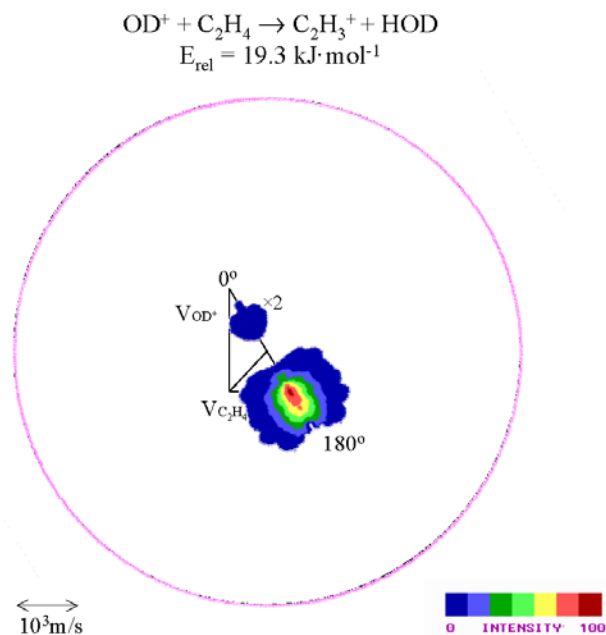


Figure 3. Contour plot representation of the C_2H_3^+ product flux at a collision energy of 19.3 kJ mol^{-1} superimposed on the Newton diagram, lowest collision energy. The circle on the contour map defines the maximum C_2H_3^+ product velocity allowed by energy conservation. Reprinted from [23] with permission from Elsevier.

5. The $\text{D}_2\text{O}^+ + \text{C}_2\text{H}_4$ system

A detailed discussion of the intermediates in this system has already appeared in the literature, so the present discussion will focus on the pathway for deuterium ion transfer to produce $\text{C}_2\text{H}_4\text{D}^+$. Figure 6 shows a reaction coordinate diagram based on the structures resulting from the DFT calculations reported in the literature [22]. Structures 1 and 4 are electrostatic complexes formed when the oxygen atom in D_2O^+ approaches a carbon or hydrogen atom in ethylene, and are precursors to charge transfer. The calculations reveal that formation of the $\text{C}_2\text{H}_4\text{D}^+$ product is controlled by a bound intermediate, denoted as structure 2 in figure 6, that is formed when one of the D atoms in D_2O^+ approaches the π -electron cloud on ethylene along the C–C perpendicular bisector. This complex lies $\sim 145 \text{ kJ mol}^{-1}$ below the approaching reactants. This complex is characterized by incipient deuterium ion transfer, ultimately yielding the bridged ethyl cation by simple O–D bond cleavage. The incipient C–D bonds associated with the bridged structure are elongated relative to their equilibrium distances in the $\text{C}_2\text{H}_4\text{D}^+$ product, consistent with the formation of products with significant vibrational excitation in the mode in which the bridging D atom moves along a coordinate perpendicular to the C–C bond.

6. The $\text{OD}^+ + \text{C}_2\text{H}_4$ system

The ground state OH^+ reagent is a triplet species in which the unpaired electrons occupy two distinct nonbonding p-orbitals on the oxygen atom. The absence of an unfilled orbital on OH^+ prohibits direct transfer of a hydride ion with its pair of electrons. In a manner analogous to reactivity in the isoelectronic $\text{O}(^3\text{P}) + \text{C}_2\text{H}_4$ system [28], we expect the approaching oxygen atom in OH^+ to undergo electrophilic

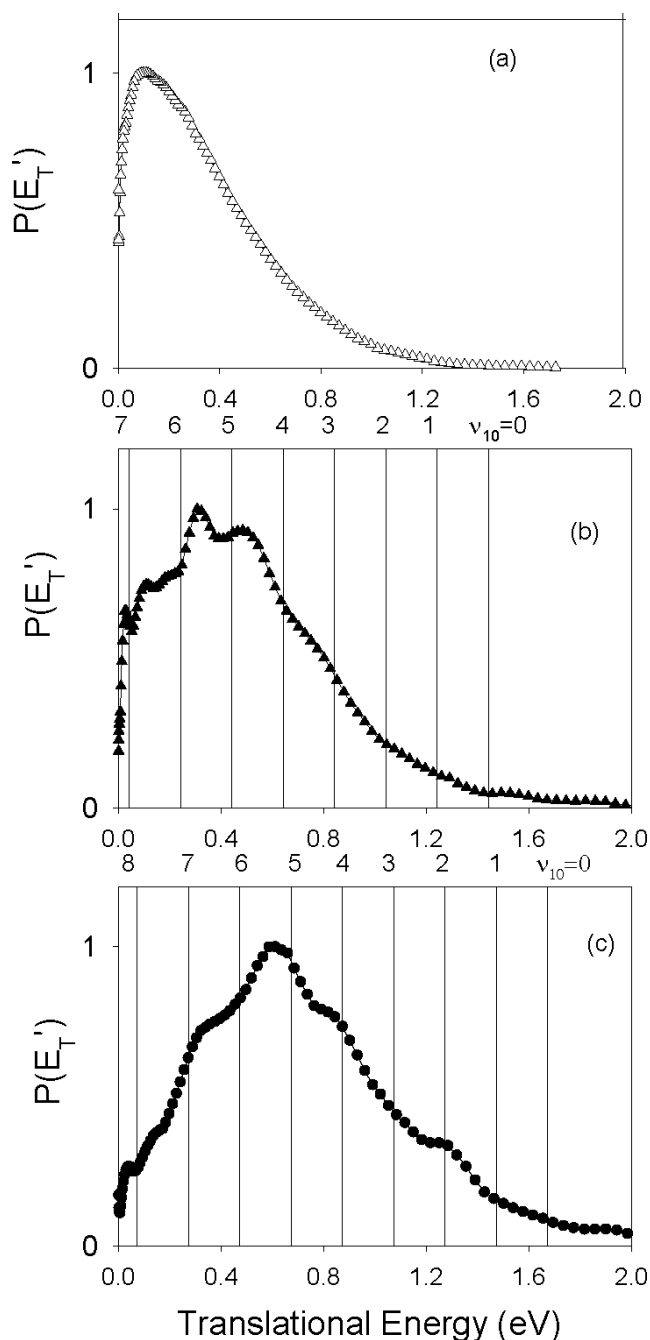


Figure 4. Panels (a)–(c): product relative kinetic energy distributions for $C_2H_4D^+$ formation, at collision energies of 0.34, 0.55 and 0.78 eV (32.8, 53.1 and 75.3 kJ mol^{-1}). Vertical lines in panels (b) and (c) correspond to product velocity corresponding to specified quanta in ν_{10} mode of a $C_2H_4D^+$ product formed with internally cold OD. Reprinted from [22] with permission of the American Institute of Physics.

addition to the π -bond of ethylene to form a triplet diradical cation species. Salem and Rowland [29] have studied such triplet diradicals; they find that when the orbitals that contain the unpaired electrons achieve an orthogonal configuration, the spin–orbit matrix elements that control intersystem crossing to the singlet manifold are nonzero. That is the case in the present system. The DFT calculations show that this triplet species lies $\sim 300 \text{ kJ mol}^{-1}$ below the reactants, and the expected facile intersystem crossing leads us to consider a reaction pathway in the singlet manifold.

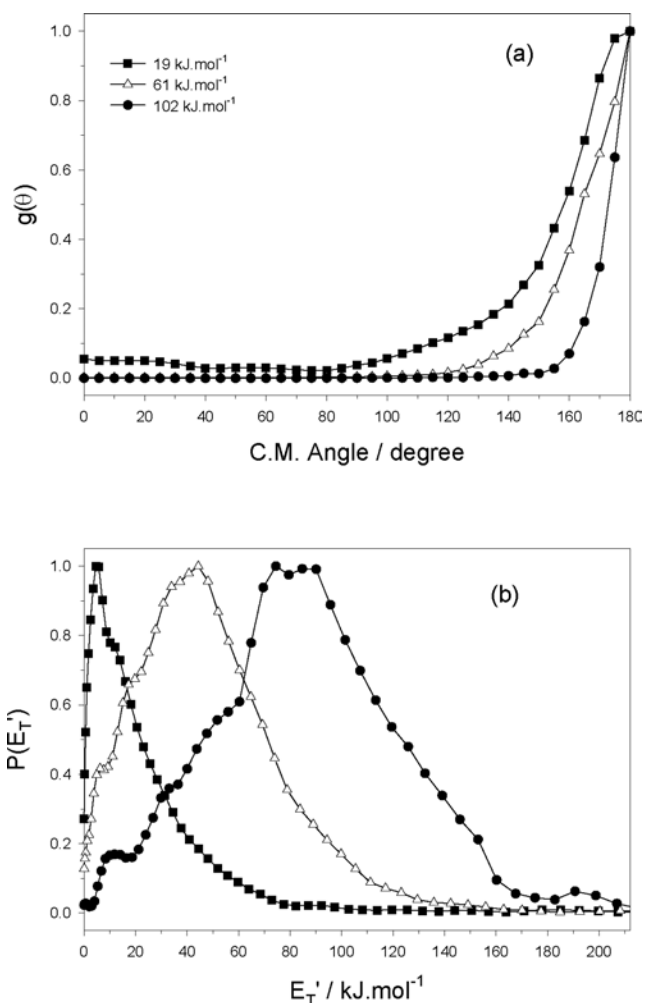


Figure 5. (a) Angular distributions for $C_2H_3^+$ hydride transfer products, all energies. (b) Kinetic energy distributions for $C_2H_3^+$ hydride transfer products, all energies. Reprinted from [23] with permission from Elsevier.

In fact, on the singlet surface, the ring-opened oxirane species is expected to close rapidly, forming protonated ethylene oxide, intermediate **1** in figure 7. In this intermediate, the hydrogen atom of the hydroxyl group is pointed out of the plane defined by the heavy atoms. The calculations show that intermediate **1** is bound by 618 kJ mol^{-1} relative to the reactants; this value compares reasonably well with a value of 643 kJ mol^{-1} evaluated from tabulated thermodynamic data. A second intermediate, denoted **2**, lies 33 kJ mol^{-1} below **1**, and is formed by cleavage of the C(1)–O bond to open the three-membered ring, followed by a hydrogen atom shift from C(2) on to the oxygen atom. The calculations are unable to identify a distinct ring-opened intermediate that precedes hydrogen atom migration; thus, the sequential motions are regarded as a single process. Intermediate **2** may undergo C–O bond cleavage through a loose transition state to form the $C_2H_3^+$ product. Isomerization of complex **1** to **2** occurs over a 140 kJ mol^{-1} barrier. We expect the rate of $\mathbf{1} \rightarrow \mathbf{2}$ interconversion to be the rate-limiting step for $C_2H_3^+$ formation.

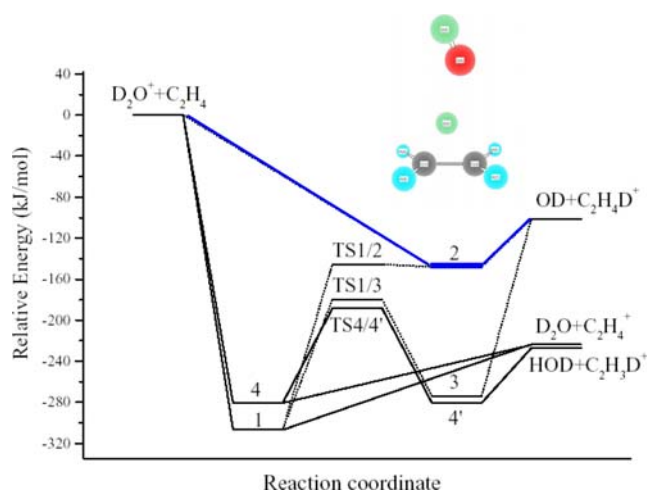


Figure 6. Schematic reaction coordinate for deuterium ion transfer in the $D_2O^+ + C_2H_4$ system. Dashed lines indicate pathways for deuterium ion transfer. The geometry of complex **2**, leading to the formation of $C_2H_5D^+$ products is shown in the diagram. Solid lines indicate pathways for charge transfer through complexes **1** and **4**, described in [22].

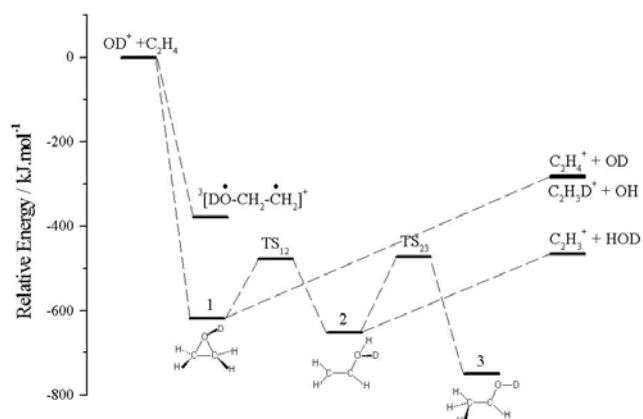


Figure 7. Schematic reaction coordinate for the $OD^+ + C_2H_4$ system. Intersystem crossing of triplet protonated oxirane to the singlet manifold precedes hydride transfer and unimolecular decay. Properties of all complexes and transition states can be found in [23].

7. Discussion

The DFT calculations show that the key reactive intermediate in the deuterium ion transfer process from D_2O^+ to C_2H_4 is the structure in which the D^+ to be transferred approaches the π -bond of ethylene along its perpendicular bisector. The nascent bridged structure of the ethyl cation is clear in the structure of this intermediate. Perhaps the most convincing experimental support for this structure comes from the nature of the kinetic energy distributions of the products at higher collision energies. The periodic structure observed in the kinetic energy distributions at the highest collision energies shows a regular spacing of 0.19 eV, which correlates with a DFT-computed frequency of 1530 cm^{-1} for the ν_{10} vibrational mode of the bridged ethyl in which the bridging D atom moves along a coordinate orthogonal to the C–C bond framework. Rotational excitation in the fragments accounts for the discrepancies between calculated and observed peak positions. This observation is an excellent

example of the synergy between calculations and experiment; the computed precursor structures exhibit distortions from product equilibrium configurations that lead to predictions of energy release in particular vibrational coordinates.

The DFT calculations also provide a natural focus for a discussion of the reaction dynamics in the $OD^+ + C_2H_4$ system. As shown in figure 7, following intersystem crossing, the singlet 1,3-diradical closes to form protonated ethylene oxide, **1**. Ring opening to structure **2** occurs through TS_{12} , a transition state with an energy of 140 kJ mol^{-1} relative to complex **1**.

The reaction coordinate for $C_2H_3^+$ formation on the singlet surface resembles double minima systems described by Brauman and Pellerite [30, 31], in which the rate-determining step is passage over the intermediate isomerization barrier, in this case TS_{12} . The DFT calculations of the vibrational frequencies of complexes **1** and **2** and the appropriate transition states allow the relevant rates to be calculated via RRKM theory. At a collision energy of 19.3 kJ mol^{-1} , the total non-fixed energies of complex **1** and the critical configuration at TS_{12} are 638 and 498 kJ mol^{-1} , respectively, and the RRKM rate for the $1 \rightarrow 2$ isomerization process is $8 \times 10^{12}\text{ s}^{-1}$. Subsequent decay of complex **2** to products by C–O bond cleavage occurs through a loose transition state with a rate constant of $1.2 \times 10^{15}\text{ s}^{-1}$. This result confirms that the rate-determining step for the formation of $C_2H_3^+$ is the interconversion for complex **1** to **2**, with a rate of $8 \times 10^{12}\text{ s}^{-1}$.

The angular distribution asymmetry observed in the $C_2H_3^+$ flux distribution at low energy provides experimental confirmation that the process to form this product is not direct, but is mediated by one or more transient intermediates. The DFT calculations show that the $1 \rightarrow 2$ isomerization process is rate limiting. Under favorable conditions, the product rotational period can serve as a ‘clock’ for a chemical reaction, and the ‘osculating model’ for chemical reactions [14, 32, 33] proceeding through complexes that live a fraction of a rotational period provides a model for extracting lifetimes. The model parameterizes the forward–backward asymmetry in the angular distribution in terms of the ratio of the complex lifetime to its rotational period, as follows:

$$g(\pi)/g(0) = \cosh(\tau_R/2\tau), \quad (5)$$

where τ is the complex lifetime and τ_R its rotational period. The low energy angular distribution shown in figure 5 suggests that $g(\pi)/g(0) \approx 10$; equation (5) thus predicts $\tau_R/\tau \approx 6$. The DFT calculation yields values of $\sim 8\text{ GHz}$ for the rotational constants of complexes **1** and **2**. Rate constant data [34] provide an estimate of the maximum impact parameter for complex formation and therefore a value of $160\hbar$ for the total angular momentum of the complex. These data yield an estimate of 700 fs for the rotational period of the complex, corresponding to a lifetime of $\sim 110\text{--}120\text{ fs}$. This result is in fortuitously good agreement with the RRKM lifetime inferred from the rate of isomerization through TS_{12} , $8 \times 10^{12}\text{ s}^{-1}$. From the perspective of rate limiting isomerization, the formation of hydride transfer products is in reasonable accord with statistical theory at the lowest collision energy.

The ability to use the rotational period of the complex as a measure of the timescale for reaction adds an

additional dimension to crossed beam experiments, which normally only probe the statistical nature of decay processes through product branching ratios and energy disposal. Such properties generally reflect the phase space accessible to reaction products, providing little information about important transition states. The observed lifetime of complex **1** depends on the properties of **TS**₁₂ and therefore provides a direct comparison with the results of RRKM calculations, and a more direct comparison with statistical theory than is provided by kinetic energy distributions alone.

8. Conclusions and outlook

The crossed beam experiments and supporting DFT calculations reported in this paper provide a very high resolution view of the reactive dynamics of the deuterium ion transfer reaction of $\text{D}_2\text{O}^+ + \text{C}_2\text{H}_4$ and the hydride ion transfer process in the $\text{OD}^+ + \text{C}_2\text{H}_4$ system. The calculations report on the role of preferred collision geometries, showing clearly that reaction (1) is mediated by an electrostatic complex in which the incipient transferred D^+ (from D_2O^+) is directed along the perpendicular bisector of the C–C bond. The elongation of the C–D bonds of the nascent cyclic $\text{C}_2\text{H}_4\text{D}^+$ product suggests that excitation of the ν_{10} vibrational mode at 1530 cm^{-1} is the preferred mode of energy disposal in this system.

In the case of the more complex $\text{OD}^+ + \text{C}_2\text{H}_4$ system, calculations suggest that intersystem crossing of the initial triplet diradical cation is rapid, and reaction occurs on the ground singlet surface. The angular distributions for product formation show that a critical intermediate decays on a timescale of ~ 120 fs, but it is the results of the calculations that allow us to assign this rate to decay of a specific complex on the ground state potential energy surface. With this identification that the isomerization of the singlet protonated ethylene oxide intermediate is rate-determining, we can make a fruitful comparison with RRKM statistical rate theory. The interplay of high resolution data from crossed beam experiments with DFT calculations of key reaction intermediates and transition states, in conjunction with RRKM-based statistical rate calculations, has provided a detailed view of the role that electrostatic and covalently bound collision complexes play in mediating ion-molecule reactions in systems of moderate molecular complexity.

The ability to provide structural characterization of reactive intermediates and transition states makes these statistical calculations, once the province of empirical correlations, now a reliable, robust procedure. More generally, with appropriate care, density functional calculations are now reliable enough to be used by experimentalists as a valuable adjunct to laboratory measurements, and systems with three and four heavy atoms can now be probed with such computations. However, theoretical advances will be necessary in making the connection between experimental data and the structure of the potential energy surface; these advances will take place in the computation of dynamics on surfaces of increasing complexity. Methods such as direct dynamics [35] will be particularly important in establishing this connection.

In addition to the challenges that theory must address, important advances must also take place in the laboratory.

Ever-higher levels of reactant state selection and product state resolution take their toll in decreased signal levels. As more complex systems are studied, both translational and optical spectroscopy face challenges as reactant and product spectra become more complex. More sensitive detection methods are called for, and the multiplex advantage afforded by velocity space imaging methods [36, 37] represents a natural dimension to explore. Finally, virtually all crossed beam studies of ion-molecule reactions have taken place with stable, closed-shell molecules. The fertile area of ion-radical reactions [38, 39] is essentially unexplored. Such systems afford new experimental and theoretical challenges: the possibility that the unpaired electron of the radical and the charge of the ion are separate entities introduces reactive intermediates that are distonic ions. The production of stable free radical sources, in conjunction with the high sensitivity and multiplex advantage of velocity space imaging methods, augurs well for future studies of new chemical systems. With the possibility that these species can be characterized by quantum chemical calculations, the synergy between theory and experiment can only grow. We look forward to these advances.

References

- [1] Su T and Bowers M T (eds) 1979 *Gas Phase Ion Chemistry* vol 1 (New York: Academic) p 83
- [2] Polanyi J C 1972 *Acc. Chem. Res.* **5** 161
- [3] Balucani N, Capozza G, Leonori F, Segoloni E and Casavecchia P 2006 *Int. Rev. Phys. Chem.* **25** 109
- [4] Casavecchia P 2000 *Rep. Prog. Phys.* **63** 355
- [5] Casavecchia P, Balucani N and Volpi G G 1999 *Ann. Rev. Phys. Chem.* **50** 347
- [6] Strazisar B R, Lin C and Davis H F 2000 *Science* **290** 958
- [7] Picconatto C A, Srivastava A and Valentini J J 2001 *J. Chem. Phys.* **114** 4837
- [8] Hirschfelder J O 1969 *Int. J. Quantum Chem. Symp.* **3** 17
- [9] Mahan B H 1974 *J. Chem. Educ.* **51** 308
- [10] Mahan B H 1974 *J. Chem. Educ.* **51** 377
- [11] Picconatto C A, Srivastava A and Valentini J J 2001 *J. Chem. Phys.* **114** 1663
- [12] Miller W B, Safron S A and Herschbach D R 1967 *Faraday Discuss. Chem. Soc.* **44** 108
- [13] Stolte S, Proctor A E, Pope W M and Bernstein R B 1977 *J. Chem. Phys.* **66** 3468
- [14] Bullitt M K, Fisher C H and Kinsey J L 1974 *J. Chem. Phys.* **60** 478
- [15] Pechukas P, Light J C and Rankin C 1966 *J. Chem. Phys.* **44** 794
- [16] Chesnavich W J and Bowers M T 1977 *J. Chem. Phys.* **66** 2306
- [17] Farrar J M 1994 *Advances in Classical Trajectory Methods* vol 2, ed W L Hase (Greenwich, Connecticut: JAI Press) p 43
- [18] Farrar J M 2003 *The Encyclopedia of Mass Spectrometry* vol I, ed P B Armentrout (Amsterdam: Elsevier) p 158
- [19] Chupka W A and Russell M E 1968 *J. Chem. Phys.* **49** 5426
- [20] Carpenter M A and Farrar J M 1997 *J. Phys. Chem. A* **101** 6475
- [21] Carpenter M A and Farrar J M 1997 *J. Phys. Chem. A* **101** 6870
- [22] Liu L, Cai X, Li Y, O'Grady E R and Farrar J M 2004 *J. Chem. Phys.* **121** 3495
- [23] Cai X, Li Y, O'Grady E R and Farrar J M 2005 *Int. J. Mass Spectrom.* **241** 271
- [24] Varley D F, Levandier D J and Farrar J M 1992 *J. Chem. Phys.* **96** 8806
- [25] Siska P E 1973 *J. Chem. Phys.* **59** 6052
- [26] Marcus R A 1952 *J. Chem. Phys.* **20** 359

- [27] Holbrook K A, Pilling M J and Robertson S H 1996 *Unimolecular Reactions* (Chichester: Wiley)
- [28] Dupuis M, Wendolowski J J, Takada T and Lester W A Jr 1982 *J. Chem. Phys.* **76** 481
- [29] Salem L and Rowland C 1972 *Angew. Chem. Int. Edn.* **11** 92
- [30] Pellerite M J and Brauman J I 1980 *J. Am. Chem. Soc.* **102** 5993
- [31] Pellerite M J and Brauman J I 1983 *J. Am. Chem. Soc.* **105** 2672
- [32] Stolte S, Proctor A E and Bernstein R B 1976 *J. Chem. Phys.* **65** 4990
- [33] Creasy W R and Farrar J M 1987 *J. Chem. Phys.* **87** 5280
- [34] Fishman V N and Grabowski J J 1999 *J. Phys. Chem. A* **103** 4879
- [35] Hase W L, Song K H and Gordon M S 2003 *Comp. Sci. Eng.* **5** 36
- [36] Houston P L *et al* 2001 *J. Chin. Chem. Soc.* **48** 309
- [37] Chandler D W and Houston P L 1987 *J. Chem. Phys.* **87** 1445
- [38] Zhang X, Kato S, Bierbaum V M, Nimlos M R and Ellison G B 2004 *J. Phys. Chem. A* **108** 9733
- [39] Zhang X, Bierbaum V M, Ellison G B and Kato S 2004 *J. Chem. Phys.* **120** 3531